Electrochimica Acta 281 (2018) 594–600

Contents lists available at ScienceDirect

Electrochimica Acta

journal homepage: www.elsevier.com/locate/electacta

Battery and supercapacitor materials in flow cells. Electrochemical energy storage in a $LiFePO_4$/reduced graphene oxide aqueous nanofluid

Daniel Rueda-Garcia [a], Zahilia Cabán-Huertas [a], Sergi Sánchez-Ribot [a], Carlos Marchante [a], Raul Benages [a], Deepak P. Dubal [b], Omar Ayyad [c], Pedro Gómez-Romero [a, *]

[a] Catalan Institute of Nanoscience and Nanotechnology (ICN2), CSIC and BIST, Campus UAB, Bellaterra, 08193, Barcelona, Spain
[b] School of Chemical Engineering, Engineering North Building, The University of Adelaide, SA 5005, Australia
[c] Faculty of Engineering, Dept. of Materials Engineering, Al-Quds University, P.O. Box 20002, East Jerusalem, Palestine

ARTICLE INFO

Article history:
Received 29 December 2017
Received in revised form
22 May 2018
Accepted 23 May 2018
Available online 26 May 2018

Keywords:
Electroactive nanofluids
$LiFePO_4$
Reduced graphene oxide

ABSTRACT

Exploring conceptual frontiers between batteries, supercapacitors, redox flow batteries (RFBs) and fuel cells (FCs), we have used a battery material (i.e. $LiFePO_4$) and a supercapacitor material (i.e. graphene) in the form of nanoparticles dispersed in an aqueous electrolyte to characterize the electrochemical activity of the resulting electroactive nanofluids.

X-ray diffraction, TEM, Raman, XPS and AFM analyses were carried out to characterize the solid $LiFePO_4$ and RGO components. The corresponding electroactive nanofluids were prepared by dispersion in an aqueous Li_2SO_4 electrolyte and stabilized with Diaminobenzoic Acid (DABA). Cyclic voltammetry measurements were used to analyze their electrochemical behavior in three-electrode cells. Charge-discharge tests of the $LiFePO_4$/RGO (positive) vs. RGO (negative) nanofluids were also performed. Effective utilization of dispersed electroactive particles (ca. 100 mAh/g(LFP) at 1C) was demonstrated, which turned out to be superior to the same LFP material used as solid electrode. A charge-transfer percolation effect provided by the RGO dispersion is proposed as the mechanism for the good performance of $LiFePO_4$ (not coated with carbon!) and RGO Nanofluids. Our results constitute a first step and proof of concept of the possible application of electroactive nanofluid electrodes in alternative flow batteries.

1. Introduction

Electrochemical Energy Storage is the midst of a regenerative resurgence. Batteries, Supercapacitors (SCs), Fuel Cells (FCs) or Redox Flow Batteries (RFBs) are markedly complementary technologies and are all called to play a role within the forthcoming sustainable energy model. From load-leveling devices to wearable electronics, to the development of smart grids to electric vehicles or to renewable energy storage. Exploring conceptual frontiers between batteries, supercapacitors, redox flow batteries (RFBs) and fuel cells (FCs) could provide new opportunities to get the best of each of those technologies.

Redox Flow Batteries (RFBs) for instance could indeed be considered as laying halfway between conventional solid-electrode batteries and FCs. Unlike traditional batteries, energy density and power density are effectively detached in RFBs. Energy is proportional to the size of the external reservoirs and power to the number of cells and area of the electrodes. This technology does not suffer memory effect and benefits from a long cycle life. These are important advantages related to the fact that active materials are ions solvated in the flowing electrolyte media. On the other hand, RFBs have drawbacks like low energy density and low specific energy due to the solubility limit of the active redox species.

Different types of mechanisms have been proposed for flow cells in water and in organic media, as discussed in a very recent review [1]. All organic RFBs have been typically developed using benzoquinone and anthraquinone. Some works combining organic and inorganic solutions (for instance anthraquinone and ferricyanide as electrolytes) have been published in order to develop organic-inorganic redox flow cells. Also a combination of Li metal

* Corresponding author.
E-mail address: pedro.gomez@icn2.cat (P. Gómez-Romero).

https://doi.org/10.1016/j.electacta.2018.05.151
0013-4686/

(deposited on the anode) and an organic molecule as catholyte has been frequently used for organic – inorganic hybrid flow batteries in organic media.

In the same review [1] a full comparative discussion of the various types of flow cells is included. Concerning energy densities, flow batteries with organic molecules in aqueous media report values below 20 $Wh \cdot L^{-1}$. For hybrid organic-inorganic redox flow batteries the energy densities increase but always to values below 40 to 50 $Wh \cdot L^{-1}$ for aqueous and organic solvents respectively. The largest value of energy density reported so far (200 $Wh \cdot L^{-1}$) corresponds to a flow cell combining metallic Li anode and a TEMPO () catholythe. This device however presents serious stability problems and has only been subject to 20 cycles [1].

Among well-established systems, All-Vanadium cells constitute the most developed type of RFBs and have an energy density of 40 $Wh \cdot L^{-1}$ and a specific energy of 25 $Wh \cdot Kg^{-1}$ and operate between 1.6 V and 1.3 V [2,3]. Those values are far away from current Li-Ion Batteries (LIBs), 150–200 $Wh \cdot Kg^{-1}$ at 3.7 V [4]. Aside from the higher voltage attained in organic LIBs, the primary reason why RFBs do not achieve the energy density values of LIBs is the low concentration of active material due to limited solubility [5,6]. Furthermore, the chemical stability of the active species is limited in some cases by the enhancement of spurious reactions at high concentrations [5,7]. Finally, there is one more factor that affects both the energy and power densities of many RFBs, namely, relatively low voltages due not only to thermodynamic but also to kinetic factors, such as the high internal resistance associated to electrolyte diffusion through selective membrane separators.

The recent proposal of Semisolid Flow Batteries (SFBs) tries to solve these drawbacks by using heterogeneous mixtures of electroactive species with surfactant and carbon particles. For example, Chiang and coworkers described a so-called semi-solid lithium flow battery [8]. And Gogotsi and coworkers described a similar system for a capacitive system [9]. A so-called *flowable* carbon-electrolyte mixture was used as the active material for capacitive energy storage and was handled in a similar way to flow or semi-solid batteries. In 2014, Nair and collaborators also reported a flow capacitor device based on a graphene dispersion in organic electrolyte, with improved energy density (14.3 $W\,h\,L^{-1}$) with respect to graphite (0.422 $W\,h\,L^{-1}$) [10]. 3D interconnected hybrid materials (RGO@CS) were used to prepare an EFC. When tested as *flowable* electrodes, the composition with a 1:2 ratio of GO to CS exhibited the highest capacitance of 200 $F\,g^{-1}$ and an improved rate performance [11]. In general, this approach has been quite popular and highly concentrated semisolid catholytes based on LiCoO2, $LiNi_{0.5}Mn_{1.5}O_4$ and $Li_4Ti_5O_{12}$ suspensions, have been developed [12].

More recently, Tarascon et al. focused on the performance of a $LiFePO_4$/$LiPF_6$ EC-DMC/Li redox flowable half-cell [13]. As a result, power densities of 328 $mW\,cm^{-2}$ at 104 $mA\,cm^{-2}$ were achieved with specific energy of 50 $Wh \cdot kg^{-1}$. It is important to mention, however, the use of intermittent flow conditions with the values reported being measured under static conditions [13].

A procedure described as “intermittent flow” was used that allowed the slurry to rest on the electrodes prior to and during measurements. Under those conditions the process of cycling of the active material could be closer to that of a solid battery electrode rather than to a flowing one.

Lu et al. reported a silicon-carbon nanocomposite semi-solid anolyte, achieving a high reversible capacity (>1200 mAh g^{-1}) and stable cycle life (>100 cycles), although the experiments were also made under interment flow conditions [14].

SFBs usually need a significant amount of dispersed conducting particles such as carbon particles, which can transform the electrolyte solution into a slurry electrode that allows for electrical conduction by percolation in all the volume of the electrode [9]. On the other hand, these conducting particles often need a surfactant to generate a stable dispersion [15]. This large amount of carbon particles and the use of surfactant are responsible for a detrimental increase in the viscosity of semisolid electrodes. Finally, the nature of the carbon used is another crucial point since it determines the electrical conductivity and thus the effectiveness of the percolation effect [16,17].

High viscosity is not compatible with flow cells, which need a pumping system to flow the solutions from the reservoirs to the electrochemical cell and vice versa, with a corresponding decrease in overall efficiency. Thus, a significant increase in viscosity of the fluids is highly undesirable, because the extra energy needed to circulate the pastes could cancel out the possible intrinsic advantages of the active materials, or at least reduce dramatically the overall efficiency of the system.

On the other hand, a different approach to the harnessing of electroactive solid particles in flow cells has been proposed by Grätzel and collaborators by introducing the concept of shuttle redox molecular solutions with suitable redox potentials, solubility, stability and kinetics to transfer the charge to solid particles stored in a separate reservoir [18].

Other approach using nanofluids was proposed by Timofeeva and col. in 2015. They developed a scalable one-step surface modification procedure for functionalizing TiO_2 nanoparticles with a monolayer coverage of propyl sulfonate groups [19]. With this new formulation the nanofluids had a high solid loading and low viscosity, while retaining the surface activity of nanoparticles.

Our approach has been to use graphene instead of activated carbon as the key material to provide an electrical percolation effect on the solution. This approach is backed by preliminary results showing extraordinary charge percolation even in dilute graphene nanofluids [20]. Thus, a stabilized dispersion of RGO in aqueous sulfuric acid solution can provide energy storage capacities similar to those of solid electrode supercapacitors (169 $F\,g^{-1}$(RGO)) but working up to much faster rates (from 1 $mV\,s^{-1}$ to the highest scan rate of 10 $V\,s^{-1}$) in nanofluids [20].

Our efforts to create graphene-based nanofluids led to the development of two new hybrid materials (rGO-phosphomolybdate, rGO-PMo_{12} and rGO-phosphotungstate, rGO-PW_{12}), dispersed with the aid of a surfactant in 1 M H_2SO_4 aqueous electrolyte to yield highly stable hybrid electroactive nanofluids (HENFs) of low viscosity which were tested in a home-made flow cell under static and continuous flowing conditions. Remarkably, even low concentration rGO-POMs HENFs (0.025 wt%) exhibited high specific capacitances of 273 F/g(rGO-PW12) and 305 F/g(rGO-PMo12) with high specific energy and specific power per mass of active material [21].

Indeed, RGO must be properly dispersed in electrolytes in order to be used as a nanofluid. This has been attempted both in aqueous and organic solvents. For example Xu et al. reported a successful production of stable high-concentration graphene dispersions in low-boiling-point, low-polarity conventional organic solvents by liquid-phase noncovalent exfoliation of graphite assisted using polyethylene (HDPE) as the stabilizer [22]. Other example of RGO dispersion, this time in water, is the report of an imidazolium-modified hexa-*peri*-hexabenzocoronene derivative (HBC-C_{11}-MIM[Cl^-] [5]) designed and synthesized as a stabilizer to disperse RGO. The resulting RGO/HBC-C_{11}-MIM[Cl^-] hybrid can reach stable concentrations of 5.0 $mg\,mL^{-1}$ (RGO) in water [23]. In these two examples the stabilization of the RGO is achieved by a solvated aromatic molecule that keeps RGO in suspension.

On the other hand, $LiFePO_4$ has been intensely studied as cathode material for LIBs since the seminal work of Goodenough in 1997 [24]. It has made it from the labs to the market thanks to its

low cost, abundant raw materials, safety, low toxicity, structural stability and excellent electrochemical properties. The active material can be reversibly charged and discharged with a stable voltage at 3.45 V vs. Li^+/Li with a very small change in unit cell parameters during the $LiFePO_4/FePO_4$ phase transition. It needs, however, conducting additives or coatings in order to display its full potential. As part of the extensive research on $LiFePO_4$ Bonaccorso, reported a battery with a graphene and $LiFePO_4$ electrodes and an energy density of 190 $Wh \cdot Kg^{-1}$ [25].

In this work we want to demonstrate the feasibility of reversibly transferring charge to/from nanoparticles of an electroactive phase (in this case, model LiFePO4) dispersed in an electrolyte by means of the presence of rGO in a stabilized nanofluid, with rGO providing effective charge percolation.

In this work, we have used 3,4-diaminobenzoic acid (DABA) to generate a stable RGO dispersion in water and lithium iron phosphate ($LiFePO_4$) nanoparticles with a 2D layered morphology to demonstrate the high rate of charge transfer throughout the graphene dispersion in low concentration and in the absence of conventional surfactants. Just small amounts of RGO dispersed in aqueous Li_2SO_4 electrolyte lead to nanofluids with low viscosity while allowing effective charge/discharge of redox $LiFePO_4$ nanoparticles.

2. Experimental section

2.1. $LiFePO_4$ synthesis

$LiFePO_4$ sample was prepared by a reflux method. Stoichiometric amounts (0.03 mmol) of $Li(CH_3COO) \cdot 2H_2O$ (3.0606 g), $Fe(CO_2CO_2) \cdot 2H_2O$ (5.3907 g) and 85 %v/v H_3PO_4 (2.05 mL) were dissolved in 70 mL of ethylene glycol. The liquid reaction mixture was placed in a round-bottom flask connected to a condenser and refluxed vigorously for 72 h at 200 °C. The final pH of this solution was 7. The resulting solid was filtered-off, washed several times with deionized water and then ethanol. The sample was dried under vacuum at 80 °C overnight, preheated at 350 °C for 5 h and then sintered at 700 °C for 10 h under nitrogen atmosphere. We collected 3.4214 g of green powder which amounts to 92% yield.

2.2. RGO synthesis

Graphite oxide (GO) was prepared from natural graphite using a modified Hummers method as follows [38]: NaNO3 (5 g) and H2SO4 (225 mL) were added to graphite (5 g) and stirred for 30 min in an ice bath. KMnO4 (25 g) was added to the resulting solution, and then the solution was stirred at 50 °C for 2 h. Deionized (DI) water (500 mL) and H2O2 (30 mL, 35%) were then slowly added to the solution. Concentrated HCl (500 mL, 37%) was added and then a final washing with 750 mL of 10% HCl, followed by dialysis until pH 6–7 and a final drying under vacuum at 70 °C, afforded the GO product as a powder. The amount of powder recovered was 4.1381 g, which represents a 16% yield. Reduced graphene oxide (RGO) was prepared by high temperature treatment of this GO sample at 800 °C under N2 atmosphere for 1 h.

2.3. Electroactive nanofluids preparation

The electroactive nanofluids discussed in this article were prepared using 1 M solutions of $Li_2SO_4 \cdot H_2O$ as base fluid and different DABA concentrations. RGO was then dispersed in this electrolyte solution, and sonicated for 5 min. The mass ratio of DABA to RGO was optimized in order to get a stable dispersion with a maximum amount of RGO. It is important to mention that pH 7 is needed for these electroactive nanofluids. To adjust the pH, $LiOH \cdot H_2O$ was added before adding $LiFePO_4$. Finally, layered $LiFePO_4$ was added and the mixture sonicated for 35 min. Different amounts of RGO and $LiFePO_4$ were tested and will be discussed through the article.

The viscosity for (DABA/RGO (40:1)) nanofluid is 1.055 (10) mPa·s at 20.1 °C. This value is very similar to the viscosity of water at the same temperature (1.002 mPa s). The electroactive nanofluid based on sample e $LiFePO_4$ 1.4 g L^{-1} (DABA/RGO (40:1)) has a viscosity of 1.72 mPa s, at 20.1 °C with a shear rate of 2880 s-1. This electroactive nanofluid has a higher viscosity than water and the base nanofluid, the higher viscosity is a result of the addition of the $LiFePO_4$ particles. However, this value is still reasonably low and perfectly compatible with low-energy pumping in a flow cell system.

2.4. Materials characterization

Physical Characterization. The phase purity and crystal structure of the samples were confirmed by X-ray diffraction (XRD) using PANalytical X'Pert PRO diffractometer using a Cu Kα radiation source ($\lambda = 1.5418$ Å) in the angular range $10° \leq 2\theta \leq 70°$ at a scan rate of 0.017° per second. The morphology of the particles was studied by Scanning Electron Microscopy (SEM) and Transmission Electron Microscopy (TEM, Tecnai G2 F20 HRTEM) operated at an acceleration voltage of 200 keV. For TEM studies, samples were dispersed in absolute ethanol, and a drop was then put onto a holey carbon coated Cu grid and allowed to evaporate slowly under ambient conditions before being introduced for TEM characterization. Raman scattering (RS) spectra were recorded on a HORIBA Scientific LabRAM HR Raman spectrometer system using Ar laser. Rheology experiments were made in the Institute de Ciencia de Materials de Barcelona (ICMAB) with a Haake RheoStress 600.

2.5. Nanofluids electrochemical test

Cyclic voltammograms were carried out from −0.2 V to 1.2 V vs Ag/AgCl 3.5 M KCl. Pt was used as counter and working electrode during the electrochemical tests of the nanofluids. Potentiostatic electrochemical impedance spectroscopy (PEIS) experiments were carried out over a frequency range of 5000 kHz and 100000 mHz, with an amplitude of 10 mV. Before the PEIS experiments, the cell was keep at constant voltage for 10 min. The voltages of the experiments were 0.0 V vs. Ag/AgCl or 0.9 V vs. Ag/AgCl the electrochemical tests were carried out with a Biologic VMP3 potentiostat/galvanostat.

2.6. Electrochemical cell

A commercial Electrolysis Cell was used (BASi Bulk). A container with a porous glass frit of 4–6 μm pore diameter was used for the charge and discharge test. In the glass frit only 1.4 g L^{-1} of $LiFePO_4$ DABA/RGO (40:1) nanofluid was placed. A DBA-RGO (40:1) dispersion was used as counter electrode in the 75 mL glass cell with an Ag/AgCl KCl 3.5 M reference electrode immersed in it (See Supplementary material). The cell was cycled between −0.2 V and 1 V vs. Ag/AgCL KCl 3.5 M at 1C. The dispersion was stirred during the experiment. It is important to mention that we balanced the amounts of active materials in each nanofluid electrode (1.4 g L^{-1} of $LiFePO_4$ DABA/RGO (40:1) sample and the DABA/RGO (40:1) sample) to balance their charge. For instance, we used 75 mL of DABA/RGO (40:1) nanofluid and 1.3 mL of the $LiFePO_4$ DABA/RGO nanofluid. The calculation was based on data from Fig. S5 (Supplementary material).

3. Results

The basic characterization of the starting materials, i.e. $LiFePO_4$ and RGO is detailed in the Supplementary Information.

3.1. Electroactive nanofluids

Behera et al. have reported that reduced graphene oxide has a better dispersibility in a pH range of 7–11 [26]. Guyomard and collaborators reported that $LiFePO_4$ has an initial pH near 7 in a water dispersion; they conclude that the stability and the electrochemical performance is better when the initial pH is not altered [27]. Furthermore, DABA solubility has a strong dependence on the pH, with decreased solubilities in acidic media (Table 1 and Table S1) probably due to the protonation of its carboxylic acid moiety. Therefore, $LiOH \cdot H_2O$ was used in order to adjust the pH at 7; this compound was selected to avoid the presence of other ions in solution.

As a preliminary step for the formulation of our final nanofluids, we optimized the DBA/RGO concentration in aqueous media. Three different DABA/RGO mass ratios were tested: 20:1, 30:1 and 40:1 (see Table 1 for concentration). As it is shown in Table 1, the more stable dispersion of DABA and RGO was the one with the mass ratio DABA/RGO 40 to 1.

For comparison, pure RGO was dispersed in the Li_2SO_4 aqueous electrolyte at a nominal concentration of 0.29 g L^{-1}. However, at this concentration RGO precipitates immediately, although a grey-colored dispersion was maintained (Table 2). This means that, although some graphene flakes remain in solution thanks to the polar oxygen groups remaining in the structure of Reduced Graphene Oxide, in the absence of DABA, the solubility limit for RGO is much lower.

The stabilization of RGO by DABA could be explained through solvation by this aromatic molecule that keeps RGO in suspension by π-π interactions, with the introduction of functional groups providing a steric effect that maintains the RGO layers apart. Indeed, DABA is an amphiphilic molecule with an aromatic core and polar groups. This must be at the heart of its capacity to stabilize RGO in water. The fact that a large excess of molecules are needed for this suggest that a simple single-layer coating of both sides of RGO sheets by DABA is not enough to explain this stabilization. Instead, we propose a multilayer structure of DABA molecules with orientations parallel to RGO sheets in the first-layer sphere (with π-π interactions) turning into loosely perpendicular orientations after a few DABA layers, with carboxylate and −NH2 groups hydrogen-bonding water molecules. Of course, this appealing hypothesis would need to be confirmed by further studies, possibly through molecular simulation.

After optimization of the DABA/RGO ratio (optimal mass ratio 40:1 DABA/RGO), we proceeded to develop an electroactive nanofluid incorporating platelet $LiFePO_4$ as redox electroactive species to test the RGO/DABA dispersion. Different amounts of $LiFePO_4$ were tested to optimize the amount of redox active material load in the nanofluid (Table 2). The sample with 0.4 g L^{-1} of $LiFePO_4$ was the most stable, however samples containing 1 g L^{-1} and 1.4 g L^{-1} of $LiFePO_4$ exhibited a stability that could be considered good enough to develop a nanofluid. Unfortunately, the sample with 2 g L^{-1} of $LiFePO_4$ layer did not show good stability. Depending on the particle concentration and the strength of particle–particle interactions, a dispersion/agglomeration equilibrium is established in the particle suspension. Large concentrations of $LiFePO_4$ platelets induce agglomeration and precipitation. On the other hand, it should be noted that even gentle stirring prevents precipitation of these more concentrated nanofluids.

Table 1
DABA experimental solubility.

DABA concentration	$LiOH \cdot H_2O$	pH	Solubility
12 g L^{-1}	N/A	4	no
12 g L^{-1}	1.6 g L^{-1}	6	partially
12 g L^{-1}	2.8 g L^{-1}	7	yes
12 g L^{-1}	3.6 g L^{-1}	10	yes

The electrochemical characterization of optimized nanofluids included cyclic voltammetry (CV) and impedance (PEIS) studies, as well as Galvanostatic Charge-Discharge (GCD) tests. As shown in Fig. 1 a, the CV of DABA shows an important change on its electrochemical signal when RGO is added. DABA alone did not show any special electrochemical response. There is an apparent wave at both ends of the selected scan range, the separation between the peaks is ca. 0.7 V vs. Ag/AgCl. The difference between these Ep_a and Ep_c, is a useful diagnostic test of a Nernstian reaction. In this case it is quite far from the value of 0.059 V at 25 °C [28] expected for a reversible reaction.

But the addition of RGO leads to the appearance of an oxidation wave at 0.3 V vs Ag/AgCl. Thus, RGO seems to promote an irreversible oxidation process. It is important to mention that the RGO dispersion shows a capacitive behavior rather than a faradaic redox process, Fig. 2 a.

Fig. 1 b shows cyclic voltammograms of nanofluids with various $LiFePO_4$ concentrations with DABA/RGO as additive at constant concentration (40/1 mass ratio). They show the expected $LiFePO_4$ redox waves at 0.65 V vs Ag/AgCl and 0.19 V vs. Ag/AgCl with intensities increasing as $LiFePO_4$ concentration increases up to 1.4 g L^{-1}. The acknowledged redox process for $LiFePO_4$ is the following [24,29]:

$$LiFePO_4 \leftrightharpoons Li^+ + e^- + FePO_4 \quad (1)$$

Finally, a redox wave associated to DABA was also detected at 0.3 V vs Ag/AgCl.

The sample with 1.4 g L^{-1} of $LiFePO_4$ led to the best electrochemical performance, although its dispersion in the nanofluid is not as long-lasting as that of more dilute sample (i.e. 0.4 g L^{-1}). Thus, the 1.4 g L^{-1} was further used to explore in detail the electrochemical characteristics of these nanofluids. The decrease in the current intensity for the nanofluid with a $LiFePO_4$ concentration of 2 g L^{-1} is a result of a co-precipitation of RGO and $LiFePO_4$ nanoparticles.

Fig. 1 c shows the electrochemical behavior of the selected sample (1.4 g L^{-1} LiFePO4 nanofluid) at different scan rates. The intensity of the Fe(II)/Fe(III) peak from $LiFePO_4$ increases as the scan rate is increased. On the other hand, the peak corresponding to DABA appears as a shoulder at low scan rates and nearly disappears as the scan rate is increased up to 25 mV s^{-1}. It should be noted that the order for recording these CVs was from fastest to slowest. Thus, the disappearance of the DABA signal cannot be due to full consumption of the chemical. Instead, it can be attribute to a slow kinetic of the DABA reaction. This observation allows us to conclude that at fast scan rates this reaction does not contribute significantly to the electrochemistry of this system. The concentration of $LiFePO_4$ also has an effect. Thus, as we can see in Fig. 3, the CV of the sample with 1 g L^{-1} of $LiFePO_4$ at 25 mV s^{-1} shows a small peak corresponding to DABA oxidation. These experiments show a decrease of the DABA signal induced both by the addition of $LiFePO_4$ and by an increase of the scan rate. That behavior suggests that the electrochemical redox processes of $LiFePO_4$ are much faster than the oxidation of DABA.

On the other hand, it is well known that $LiFePO_4$ electroactivity is hindered by its poor electronic conductivity (10^{-9} S cm^{-1}) and

Table 2
Stability of the nanofluids (12 mg/mL DABA, 2.8 mg/mL $LiOH.H_2O$, 1 M of $Li_2SO_4H_2O$, pH 7).

Sample	Aspect	Stability	Complete precipitation of the dispersion (hours)
RGO (0.29 ng/L)	Translucent grey	immediate	N/A
Diaminobenzoic acid/RGO **(20:1)** (0.6 g L^{-1} RGO)	Translucent	Precipitation starts after 4 h.	7
Diaminobenzoic acid/RGO **(30:1)** (0.4 g L^{-1} RGO)	(orange) Decrease with time	Precipitation starts after 27 h.	56
Diaminobenzoic acid/RGO **(40:1)** (0.3 g L^{-1} RGO)	(orange) Decrease with time	Precipitation starts after 97 h.	120
Diaminobenzoic acid/RGO (40:1)/**0.4 g L^{-1} $LiFePO_4$**	Brown	Precipitation starts after ca. 24 h	36
Diaminobenzoic acid/RGO (40:1)/**1 g L^{-1} $LiFePO_4$**	Almost Black	N/A	Around 24
Diaminobenzoic acid/RGO (40:1)/**1.4 g L^{-1} $LiFePO_4$**	Almost black	N/A	Around 24
Diaminobenzoic acid/RGO (40:1)/**2 g L^{-1} $LiFePO_4$**	Black	N/A	More than 12 less than 24

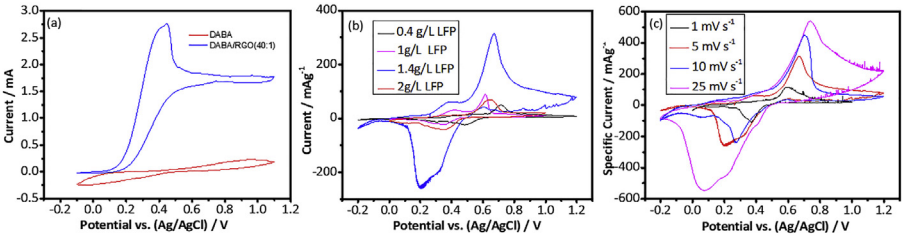

Fig. 1. (a) Cyclic Voltammograms of DABA (12 g L^{-1}) (red trace) and DABA/RGO (12 g L^{-1} and 0.3 g L^{-1} respectively) (blue) showing a characteristic irreversible oxidation wave of DABA enabled by RGO. Scan rate 5 mV s^{-1} (b) Cyclic Voltammograms of $LiFePO_4$ (DABA-RGO (40/1)) (concentrations of $LiFePO_4$ 0.4 g L^{-1}, 1 g L^{-1}, 1.4 g L^{-1}, 2 g L^{-1}). Scan rate 5 mV s^{-1}. (c) Cyclic Voltammetry at different scan rates of $LiFePO_4$ (1.4 g L^{-1}). Inset shows the CV of a 1 g L^{-1} $LiFePO_4$ in DABA/RGO (40/1) in which the characteristic wave from DABA is still apparent. (For interpretation of the references to colour in this figure legend, the reader is referred to the web version of this article.)

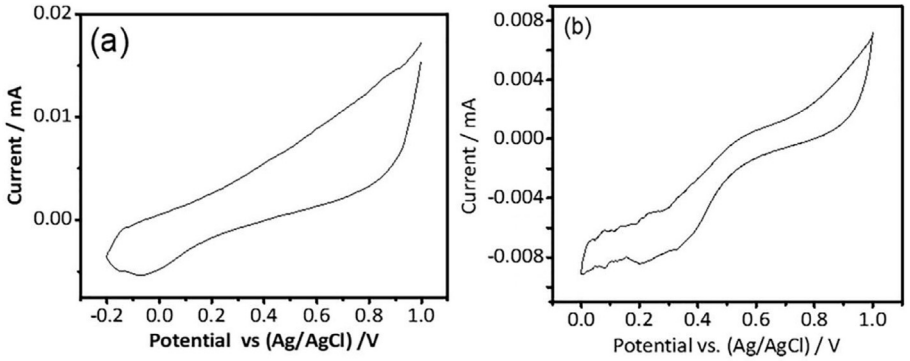

Fig. 2. Cyclic voltammogram of (a) RGO (b) 1.4 g L^{-1} of $LiFePO_4$ in an aqueous electrolyte The electrolyte is 1 M Li_2SO_4 with 1.4 gL^{-1} of $LiFePO_4$. The scan rate was 5 mVs^{-1}.

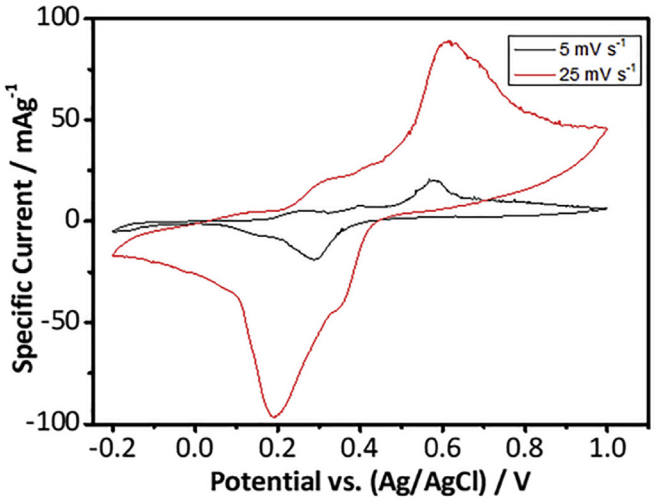

Fig. 3. Cyclic voltammogram of 1 g L^{-1} of $LiFePO_4$ in DABA/RGO (40:1).

slow lithium diffusion [30]. Increasing the conductivity by coating the $LiFePO_4$ surface with carbon [29,31] or conducting polymers [32,33] have been two of the most popular approaches to improve the capacity and rate performance of $LiFePO_4$ in LIBs. Similarly, our experiments show that in the absence of RGO the Cyclic Voltammogram of $LiFePO_4$ does not show a well-defined electrochemical signal (Fig. 2 b). This behavior changes dramatically when the nanofluid contains DABA-stabilized RGO in addition to $LiFePO_4$, with well-defined and intense redox peaks unambiguously assigned to $LiFePO_4$ (Fig. 3). This indicates that the water-dispersed RGO allows for an effective charge-transfer percolation between the current collector and the uncoated $LiFePO_4$ nanosheets.

PEIS experiments were carried out for the 1.4 g L^{-1} $LiFePO_4$ nanofluid and the corresponding Nyquist plots for the system in its reduced (0.0 V vs. Ag/AgCl) (Fig. 4 a) and oxidized (0.9 V) (Fig. 4 b) states. The results fit the Randles equivalent circuit (inset Fig. 4 b) typical for a simple electrochemical process. In this equivalent circuit, there is a resistance associated to the electrolyte and the external circuit, which in the Nyquist plot corresponds to the point in the real axes where the semicircle begins. This point is the same

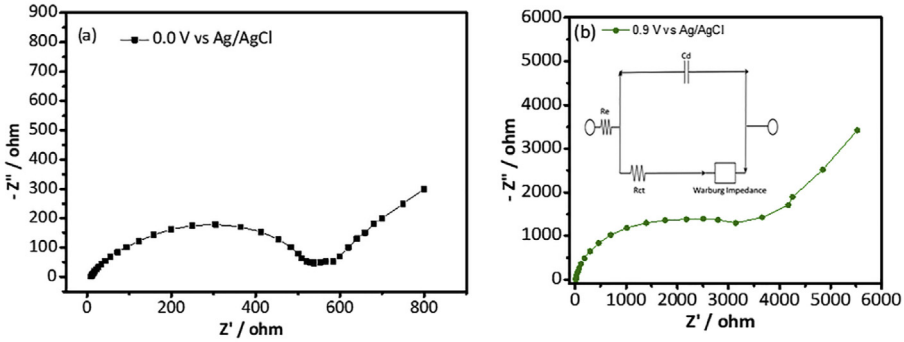

Fig. 4. PEIS impedance spectra of $LiFePO_4$ (1.4 g L^{-1}) in DABA/RGO (40:1) (a) recorded at 0.0 V (reduced) and (b) at 0.9 V (oxidized).

for the oxidation and reduction processes of the sample. The value of this resistance is negligible compared to the resistance associated with the charge transfer, discussed below.

The charge transfer resistance related to the redox process can be measured by the width of the semicircle observed in the real axes of the Nyquist plot. The semicircle is larger for the oxidation than for the reduction process in $LiFePO_4$. This agrees with other publications, where they found that $LiFePO_4$ is more stable than $FePO_4$ [34]. This also means that the de-intercalation process is less favorable than the intercalation process in this system.

The inclined line in the low frequency zone of the plot represents the Warburg impedance (Z w), which is customarily associated to lithium-ion diffusion in the material [35]. This process is associated with a mass transfer control.

Fig. 5 a shows the performance of a full cell with the $LiFePO_4$ (1.4 g L^{-1}) -DABA/RGO (40:1) nanofluid as positive electrode and the DABA/RGO (40:1) nanofluid as negative electrode cycled at 1C. The discharge capacity of the cell is ca. 140 mA h g^{-1}($LiFePO_4$) at 1 C.

The Coulombic efficiency of the cell increases continuously from 65% (1st cycle) up to ca. 90% (5th cycle). This is not an intrinsic behavior of the electroactive phases in the nanofluids. We believe the initial lower efficiency could be related to some irreversible (but minor) reaction taking place during the first few cycles of charge. Finally, the results show a high utilization of the $LiFePO_4$.

Fig. 5 b shows a plot of the potential of the working electrode vs. capacity for a single representative cycle (5th cycle). The charge capacity is only slightly larger than the discharge capacity, in agreement with the evolution of the coulombic efficiency shown in Fig. 4 a. The profile of the cell shows a clear plateau around 0.35 V (discharge) and 0.55 V (charge) vs Ag/AgCl.

4. Conclusions

We successfully developed a stable dispersion of RGO in water thanks to the addition of DiAminoBenzoic Acid (DABA). This aromatic but polar molecule interacts with RGO through π-π forces equivalent to a solvating effect. As a consequence of this interaction RGO was maintained in water as stable dispersions. Furthermore, the steric effect of the functional groups of the DABA preclude the restacking of RGO layers, which remain separated in the dispersion.

Our results show the strong effect of adding RGO-DABA to a nanofluid containing $LiFePO_4$ allowing for an effective charge-transfer percolation between the current collector and the uncoated $LiFePO_4$ nanosheets. The latter were used as a model electroactive nanoparticulate phase and showed an improvement of its redox performance in the nanofluid with respect to their use in a solid electrode. It should also be noted that our base nanofluid (RGO-DABA) does not disturb the electrochemical signal of this $LiFePO_4$, despite the enhancement by RGO of a redox process of DABA (not observed with pristine DABA). In this respect, we must conclude that the relatively much faster and reversible $LiFePO_4$ electrochemistry precludes the process of irreversible oxidation of DABA, especially at fast rates. Finally, our work shows how to harness the electroactivity of $LiFePO_4$ integrated in a freely flowing nanofluid. It should be noted that $LiFePO_4$ nanosheets in the nanofluid where not coated with any conducting material. Yet, they performed better than similarly uncoated nanoparticles integrated in a conventional electrode. This improved performance must be assigned to the efficient charge-transfer from current collectors mediated by RGO in the nanofluid.

We feel our present work represents one end of a research line connecting i) well-dispersed nanofluids (sols) with low viscosity but low energy density (this work) and ii) the many paste

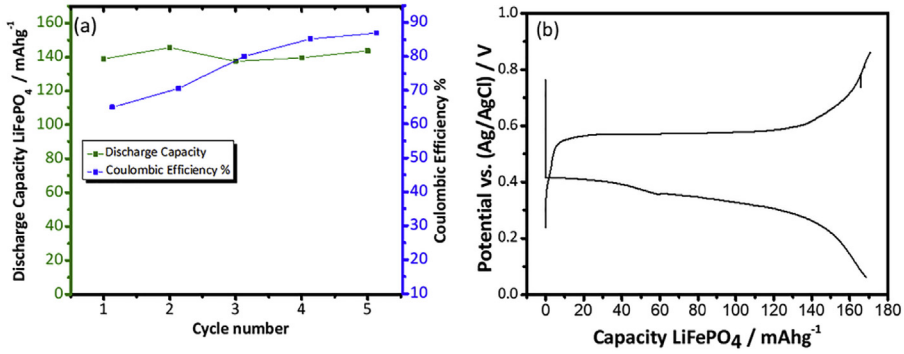

Fig. 5. (a) Evolution of discharge capacity and coulombic efficiency of a two-nanofluid cell with $LiFePO_4$ (1.4 g L^{-1})-DABA/RGO (40/1) as positive and DABA/RGO (40/1) as negative electrodes. Full cell cycled at 1C. (b) Charge and Discharge profiles (cell Voltage vs. charge) of the full Nanofluids cell.

formulations with higher energy density but poor flowing characteristics reported in the literature. It is our opinion that a whole new world of opportunities lies in between: the world of *nanopastes*, with heavy loads of solid nanoparticles dispersed in liquids, yet with the particles stabilized to avoid agglomeration, thus keeping the interface between solid and liquid domains effectively active at the nanodimension.

Acknowledgements

Partial funding from the Spanish Ministry (MINECO-FEDER MAT2015-68394-R. NaCarFLOW) and recognition from AGAUR (2017_SGR_870) are acknowledged.

The ICN2 is funded by the CERCA programme/Generalitat de Catalunya. The ICN2 is supported by the Severo Ochoa programme of the Spanish Ministry of Economy, Industry and Competitiveness (MINECO, grant no. SEV-2013-0295).

Appendix A. Supplementary data

Supplementary data related to this article can be found at https://doi.org/10.1016/j.electacta.2018.05.151.

References

[1] P. Leung, A.A. Shah, L. Sanz, C. Flox, J.R. Morante, Q. Xu, M.R. Mohamed, C. Ponce de León, F.C. Walsh, Recent developments in organic redox flow batteries: a critical review, J. Power Sources 360 (2017) 243–283.
[2] Q. Huang, Q. Wang, Next-generation, high-energy-density redox flow batteries, ChemPlusChem 80 (2015) 312–322.
[3] G.L. Soloveichik, Flow batteries: current status and trends, Chem. Rev. 115 (2015) 11533–11558.
[4] Z. Yang, J. Zhang, M.C.W. Kintner-Meyer, X. Lu, D. Choi, J.P. Lemmon, J. Liu, Electrochemical energy storage for green grid, Chem. Rev. 111 (2011) 3577–3613.
[5] L. Hoober-Burkhardt, S. Krishnamoorthy, B. Yang, A. Murali, A. Nirmalchandar, G.K.S. Prakash, S.R. Narayanan, A new Michael-reaction-resistant benzoquinone for aqueous organic redox flow batteries, J. Electrochem. Soc. 164 (2017) A600–A607.
[6] M.O. Bamgbopa, Y. Shao-Horn, S. Almheiri, The potential of non-aqueous redox flow batteries as fast-charging capable energy storage solutions: demonstration with an iron-chromium acetylacetonate chemistry, J. Mater. Chem. A 5 (2017) 13457–13468.
[7] D. Rueda-García, D.P. Dubal, F. Huguenin, P. Gómez-Romero, Hurdles to organic quinone flow cells. Electrode passivation by quinone reduction in acetonitrile Li electrolytes, J. Power Sources 350 (2017) 9–17.
[8] M. Duduta, B. Ho, V.C. Wood, P. Limthongkul, V.E. Brunini, W.C. Carter, Y.-M. Chiang, Semi-solid lithium rechargeable flow battery, Adv. Energy Mater. 1 (2011) 511–516.
[9] V. Presser, C.R. Dennison, J. Campos, K.W. Knehr, E.C. Kumbur, Y. Gogotsi, The electrochemical flow capacitor: a new concept for rapid energy storage and recovery, Adv. Energy Mater. 2 (2012) 895–902.
[10] S. Sasi, A. Murali, S.V. Nair, A.S. Nair, K.R.V. Subramanian, The effect of graphene on the performance of an electrochemical flow capacitor, J. Mater. Chem. A 3 (2015) 2717–2725.
[11] M. Boota, K.B. Hatzell, M. Alhabeb, E.C. Kumbur, Y. Gogotsi, Graphene-containing flowable electrodes for capacitive energy storage, Carbon 92 (2015) 142–149.
[12] M. Duduta, B. Ho, V.C. Wood, P. Limthongkul, V.E. Brunini, W.C. Carter, Y.M. Chiang, Semi-solid lithium rechargeable flow battery, Adv. Energy Mater. 1 (2011) 511–516.
[13] S. Hamelet, T. Tzedakis, J.-B. Leriche, S. Sailler, D. Larcher, P.-L. Taberna, P. Simon, J.-M. Tarascon, Non-aqueous Li-Based redox flow batteries, J. Electrochem. Soc. 159 (2012) A1360–A1367.
[14] H. Chen, N.-C. Lai, Y.-C. Lu, Silicon–carbon nanocomposite semi-solid negolyte and its application in redox flow batteries, Chem. Mater. 29 (2017) 7533–7542.
[15] L. Madec, M. Youssry, M. Cerbelaud, P. Soudan, D. Guyomard, B. Lestriez, Surfactant for enhanced rheological, electrical, and electrochemical performance of suspensions for semisolid redox flow batteries and supercapacitors, ChemPlusChem 80 (2015) 396–401.
[16] M. Boota, K.B. Hatzell, M. Beidaghi, C.R. Dennison, E.C. Kumbur, Y. Gogotsi, Activated carbon spheres as a flowable electrode in electrochemical flow capacitors, J. Electrochem. Soc. 161 (2014) A1078–A1083.
[17] J.W. Campos, M. Beidaghi, K.B. Hatzell, C.R. Dennison, B. Musci, V. Presser, E.C. Kumbur, Y. Gogotsi, Investigation of carbon materials for use as a flowable electrode in electrochemical flow capacitors, Electrochim. Acta 98 (2013) 123–130.
[18] Q. Huang, H. Li, M. Gratzel, Q. Wang, Reversible chemical delithiation/lithiation of LiFePO4: towards a redox flow lithium-ion battery, PCCP 15 (2013) 1793–1797.
[19] S. Sen, V. Govindarajan, C.J. Pelliccione, J. Wang, D.J. Miller, E.V. Timofeeva, Surface modification approach to TiO2 nanofluids with high particle concentration, low viscosity, and electrochemical activity, ACS Appl. Mater. Interfaces 7 (2015) 20538–20547.
[20] D.P. Dubal, P. Gomez-Romero, Electroactive graphene nanofluids for fast energy storage, 2D Mater. 3 (2016) 031004.
[21] D.P. Dubal, D. Rueda-Garcia, C. Marchante, R. Benages, P. Gomez-Romero, Hybrid Graphene-Polyoxometalates Nanofluids as Liquid Electrodes for Dual Energy Storage in Novel Flow Cells, The Chemical Record, 0.
[22] L. Xu, J.-W. McGraw, F. Gao, M. Grundy, Z. Ye, Z. Gu, J.L. Shepherd, Production of high-concentration graphene dispersions in low-boiling-point organic solvents by liquid-phase noncovalent exfoliation of graphite with a hyperbranched polyethylene and formation of graphene/ethylene copolymer composites, J. Phys. Chem. C 117 (2013) 10730–10742.
[23] H. Wei, Y.-Y. Li, J. Chen, Y. Zeng, G. Yang, Y. Li, Dispersion of reduced graphene oxide in multiple solvents with an imidazolium-modified hexa-peri-hexabenzocoronene, Chem. Asian J. 7 (2012) 2683–2689.
[24] A.K. Padhi, K.S. Nanjundaswamy, J.B. Goodenough, Phospho-olivines as positive-electrode materials for rechargeable lithium batteries, J. Electrochem. Soc. 144 (1997) 1188–1194.
[25] J. Hassoun, F. Bonaccorso, M. Agostini, M. Angelucci, M.G. Betti, R. Cingolani, M. Gemmi, C. Mariani, S. Panero, V. Pellegrini, B. Scrosati, An advanced lithium-ion battery based on a graphene anode and a lithium iron phosphate cathode, Nano Lett. 14 (2014) 4901–4906.
[26] S. Kashyap, S. Mishra, S.K. Behera, Aqueous colloidal stability of graphene oxide and chemically converted graphene, J. Nanoparticles 2014 (2014) 6.
[27] W. Porcher, P. Moreau, B. Lestriez, S. Jouanneau, D. Guyomard, Is LiFePO4 stable in Water?: toward greener Li–Ion batteries, Electrochem. Solid State Lett. 11 (2008) A4–A8.
[28] A.J. Bard, L.R. Faulkner, Electrochemical Methods: Fundamentals and Applications, Wiley, New York, 2001.
[29] Z. Cabán-Huertas, O. Ayyad, D.P. Dubal, P. Gómez-Romero, Aqueous synthesis of $LiFePO_4$ with fractal granularity, Sci. Rep. 6 (2016) 27024.
[30] Y.-N. Xu, S.-Y. Chung, J.T. Bloking, Y.-M. Chiang, W.Y. Ching, Electronic structure and electrical conductivity of undoped $LiFePO_4$, Electrochem. Solid State Lett. 7 (2004) A131–A134.
[31] N. Ravet, Y. Chouinard, J.F. Magnan, S. Besner, M. Gauthier, M. Armand, Electroactivity of natural and synthetic triphylite, J. Power Sources 97–98 (2001) 503–507.
[32] A. Fedorková, A. Nacher-Alejos, P. Gómez-Romero, R. Oriňáková, D. Kaniansky, Structural and electrochemical studies of PPy/PEG-$LiFePO_4$ cathode material for Li-ion batteries, Electrochim. Acta 55 (2010) 943–947.
[33] A.V. Murugan, T. Muraliganth, A. Manthiram, Microwave-irradiated solvothermal synthesis of $LiFePO_4$ nanorods and their nanocomposites for lithium ion batteries, ECS Trans. 16 (2009) 49–56.
[34] P. Tang, N.A.W. Holzwarth, Y.A. Du, Comparison of the electronic structures of four crystalline phases of FePO4, Phys. Rev. B 76 (2007) 174118.
[35] A. Fedorkova, R. Orinakova, A. Orinak, M. Kupkova, H.D. Wiemhofer, J.N. Audinot, J. Guillot, Electrochemical and XPS study of LiFePO4 cathode nanocomposite with PPy/PEG conductive network, Solid State Sci. 14 (2012) 1238–1243.
[38] N.J. Dudney, Thin film micro-batteries, Electrochem. Soc. Interface 17 (2008).

SUPPLEMENTARY INFORMATION

Lithium iron phosphate characterization

The $LiFePO_4$ material prepared presents the expected olivine phase as confirmed by powder XRD (Error! Reference source not found. **a**) with high purity. All diffraction peaks are indexed to orthorhombic $LiFePO_4$ (JCPDS card number 081-1173, space group Pnma), with no impurities detected. The average primary crystallite size, as determined from the peak width at 23 2Θ by the Scherrer equation, was 38 nm, substantially smaller than the average size of the plates which was found to be 138 nm.

On the other hand, the synthesis procedure reported here for $LiFePO_4$ leads to a striking, unusual morphology and agglomeration of thin plates**,** Error! Reference source not found. **b**. This sample is well crystallized, single-crystals according to their Selected Area Electron Diffraction (SAED) patterns, Error! Reference source not found. **c**. This analysis of the SAED pattern, obtained from the isolated nanoparticle shows in the inset of this figure, shows that this particle has a plane axis of [100]. The inset shows a TEM image of the particle used to obtain the SAED. The planes show by this nanoparticle can be index 101 and 020, corresponding to the bc plane. These axes are listed in a JCPDS card number 081-1173 of $LiFePO_4$**.**

In the absence of such a conducting coating, the maximum discharge capacity obtained for this material in half cells vs. Li was around 100 $mA{\cdot}h{\cdot}g^{-1}$ at 0.10C, decreasing progressively at higher rates down to 30 $mA{\cdot}h{\cdot}g^{-1}$ at 5C and ca. 10 $mA{\cdot}h{\cdot}g^{-1}$ at 10C (Error! Reference source not found. **b**).

RGO characterization

Error! Reference source not found. **a** shows micrographs of representative RGO sheets at different scales. These sheets are very thin and segregated, although their preparation for TEM results in wrinkles

and partial overlap with each other. The SAED pattern of the sheet shown in the top inset (Error! Reference source not found. **a**) shows a typical hexagonal symmetry but with strongly distorted elongated spots, which is representative of single-crystalline graphene layers with a high degree of distortions.

Raman scattering is one of the most widely used techniques to characterize the structural and electronic properties of carbon materials. **Figure S3 b** shows the Raman spectrum of our RGO with a D band at 1355.2cm^{-1} and a G band at 1595.3 cm^{-1}. The D band is related to the degree of disorder and its intensity shows the degree of edge chirality. Thus, the intensity ratio of G and D band (ID/IG) of RGO indicates the degree of the disorder. As shown in Error! Reference source not found. **b**, the ID/IG ratio of RGO is 0.99. This spectrum shows that this sample has 2 other bands at 2716.3 and 2953.9 cm^{-1}. The bands correspond to 2D (2953.9 cm^{-1}), a combination scattering peak [36, 37]; a second order overtone of a different in plane vibration D + G (2716.3 cm^{-1}).[37]

D and G Raman bands can be deconvoluted using four Gaussians or Gaussian-Lorentzian lines in order to estimate the ratio of sp^2 to sp^3 type carbon.[38] We have fitted the Raman intensity profiles using four Gaussian lines, see **Figure S3 b**, and have estimated intensity ratio Isp^2/Isp^3 = (I1270+ I1610) / (I1100+I1510). For RGO sample, we found a value for Isp^2/Isp^3 =3.2.

Electrode preparation for solid-electrode test cell

The cathodes were prepared by pressing a mixture of the active materials with Carbon Super-P (Timcal) and Polyvinylidene fluoride (PVDF) binder in a weight ratio 85/10/5. They were mixed in a mortar for 5 minutes and then dispersed in N-Methyl-2-pyrrolidone and coated onto Al foil.

Solid half cells

Electrochemical test cells (Swagelok-type) were assembled in an argon-filled glove box with the coated sample electrode as working electrode, lithium metal foil as the counter/reference electrode, and 1 M solution of $LiPF_6$ in a 1:1 vol/vol mixture of ethylene carbonate and diethyl carbonate as the electrolyte. Glass microfiber filter paper was used as separator. $LiFePO_4$ solid state half cells were subject to galvanostatic charge/discharge cycles from 2.5 V to 4.0 V at different C-rates. Cyclic voltammetry was performed (1 mV/s) in the same voltage range.

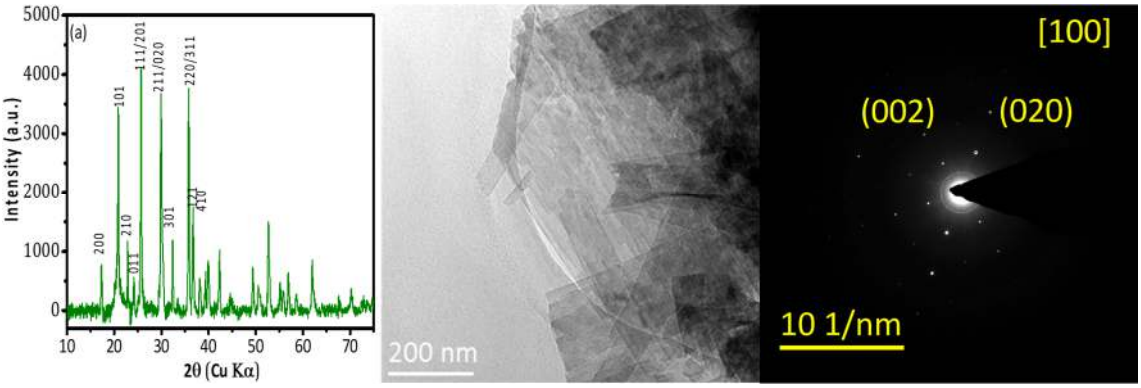

Figure S1 (a) XRD pattern (indexes shown only up to 37º) (b) TEM image showing the flake microstructure and (c) Selected Area Electron Diffraction (SAED) pattern; all corresponding to our solid $LiFePO_4$ material.

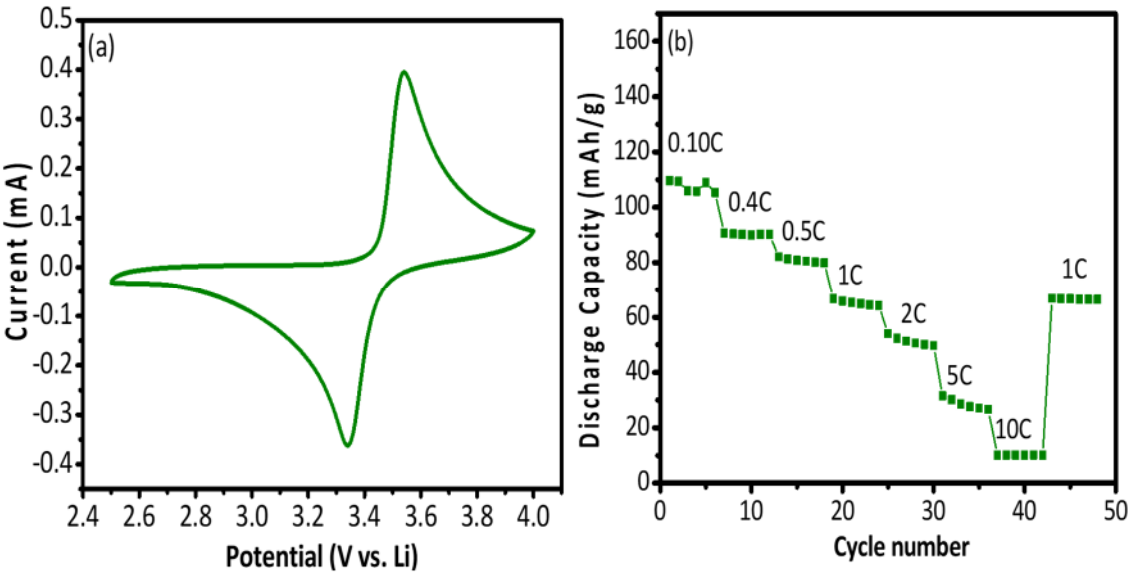

Figure S1 (a) Cyclic Voltammetry of $LiFePO_4$ scan rate 0.5 $mV \cdot s^{-1}$ (b) Rate Capability of the half-cell Li/$LiFePO_4$ from Galvanostatic Charge-Discharge measurements at various current densities.

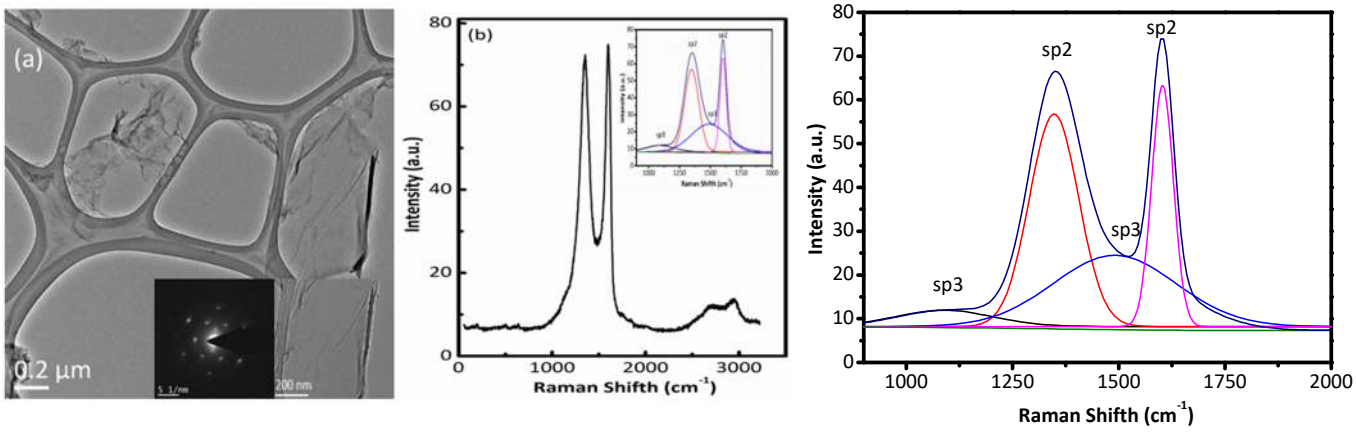

Figure S2 (a) RGO HRTEM image, inset SAED and TEM image (b) Raman spectra of GO (bottom) and RGO (top) (inset shows RGO D and G band deconvolution)

A commercial Electrolysis Cell (BASi Bulk) (**Figure S4**) was modified for our experiments. Thus, a tube with a porous glass frit of 4-6 µm pore diameter was used for the charge and discharge test. In the glass frit only 1.4 $g \cdot L^{-1}$ of $LiFePO_4$ DABA/RGO (40:1) nanofluid was placed. A DBA-RGO (40:1) dispersion was used as counter electrode in the 75 mL glass cell with Ag/AgCl KCl 3.5M as reference electrode

Figure S4 Bulk Cell model MF-1056d

For the setting up of the cell, we balanced the amounts of active materials in each nanofluid (1.4 $g \cdot L^{-1}$ of $LiFePO_4$ DABA/RGO (40:1) and DABA/RGO (40:1)) to balance their charge. Thus, we used 75 mL of DABA/RGO (40:1) nanofluid and 1.3 mL of the $LiFePO_4$ DABA/RGO nanofluid. The calculation was based on capacity data extracted from the plot in **Figure S5** below.

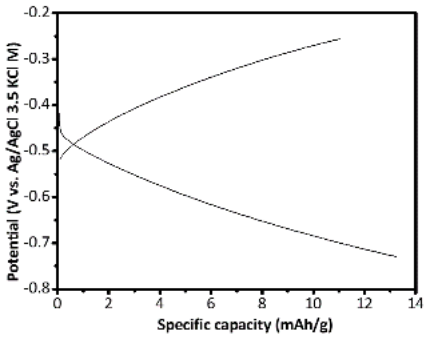

Figure S5 Capacity vs. Potential profile of symmetric capacitor cell with DABA/RGO (40:1) electrodes**.** Cycle at 500 mA for one hour. Both the anolyte and the catholyte were DABA/RGO (40:1).

Table S1 Theoretical solubility of DABA at 25 ° C [(a)]

pH	Concentration ($g \cdot L^{-1}$)
1	263
2	30
3	5.2
4	2.7
5	4
6	18
7	161
8	1000
9	1000
10	1000

(a) Calculated using Advanced Chemistry Development (ACD/Labs) Software V11.02 (© 1994-2017 ACD/Labs)